JOURNAL OF AIRCRAFT
Vol. 47, No. 3, May–June 2010

Hybrid Reynolds-Averaged Navier–Stokes and Kinetic Eddy Simulation of External and Internal Flows

Mina Zaki,* Suresh Menon,† and Lakshmi N. Sankar‡
Georgia Institute of Technology, Atlanta, Georgia 30332-0150.

DOI: 10.2514/1.43454

A hybrid Reynolds-averaged Navier–Stokes and kinetic eddy simulation turbulence model is proposed for external and internal flow applications. This hybrid Reynolds-averaged Navier–Stokes and kinetic eddy simulation model solves Menter's k-ω-SST model near walls and switches to a kinetic eddy simulation model away from walls. The kinetic eddy simulation model solves directly for local turbulent kinetic energy and local turbulent length scales, thus alleviating the grid-spacing dependency found in other detached eddy simulation and hybrid Reynolds-averaged Navier–Stokes and large eddy simulation models. Within the hybrid Reynolds-averaged Navier–Stokes and kinetic eddy simulation model, four different options (a combination of two different blending functions and the use of realizability constraints to bound the kinetic eddy simulation model parameters) have been evaluated and studied for flows over airfoils (RAE2822, NACA0015) and a turbine vane configuration. Although all four options showed good correlation with the test data, blending k-ω-SST with kinetic eddy simulation using Menter's k-ω-SST F_2 function showed better predictions in separated flows than using the baseline k-ω-SST model.

I. Introduction

MOST current computational fluid dynamics (CFD) methods used in the simulation and analysis of external and internal flows are based on Reynolds-averaged Navier–Stokes (RANS) approaches, which depend on turbulence-closure models to provide flowfield turbulent variables. Although RANS approaches yield good predictions for attached flowfields, they fail to accurately predict flow structures in separated-flow regions because they resolve only a portion of the turbulence scales of interest. Of course, the ideal approach would be direct numerical simulation (DNS), because the entire range of spatial and temporal scales of turbulence is resolved, but the computational cost of DNS is prohibitive. Another intermediate technique between DNS and RANS has been proposed to replace RANS in such cases; this approach is called large eddy simulation (LES).

In LES, the contribution of large energy-containing structures and all scales larger than the grid resolution to momentum and energy transfer is computed, and the effect of subgrid unresolved small scales is modeled. The main limitation of LES is that the wall shear layers have to be accurately resolved. To capture the near-wall flow structures in the LES approach, the distance from the wall to the first grid point should be about one wall unit ($y^+ \sim 1$) [1]. This requirement along with commencing grid spacing in the other directions gives rise to a large grid requirement and thus a prohibitive computational cost. To alleviate this grid resolution requirement, researchers have proposed using RANS in near-wall regions and use LES approach away from walls. These approaches have been called hybrid RANS/LES (HRLES) methods.

The need for different approaches for computing turbulent Reynolds stresses near the wall and away from the wall was recognized as early as the 1960s. Smith and Cebeci [2] computed eddy viscosity in the region close to the wall using Prandtl's mixing-length model while using eddy viscosity that is proportional to the product of the boundary-layer edge velocity and the displacement thickness away from the wall. This approach, called the Cebeci–Smith model, was adopted in early turbulence models for use in Navier–Stokes analyses. For example, the well-known Baldwin–Lomax model [3] uses Prandtl's mixing-length theory near walls and an approach similar to that of Cebeci–Smith elsewhere. In these models, the distance from the nearest solid walls was used to compute the model length scales.

Spalart et al. [4] realized that in free shear layers, the distance from the wall does not represent an appropriate length scale. Other length scales such as shear-layer thickness are more relevant. Inspired by ongoing research on LES, Spalart et al. extended the earlier Spalart–Allmaras (SA) model [5] so that it yielded a conventional eddy viscosity near the wall-bounded regions but switched to a pseudo Smagorinsky LES model that is proportional to the grid spacing Δ away from the wall. This approach, called detached eddy simulation (DES), was found to yield superior results compared with the earlier approaches for separated flows (e.g., static and dynamic stall). Other researchers [6–9] investigated similar concepts of DES based on two-equation turbulence models.

Other HRLES approaches have also been proposed. Speziale [10] proposed to bridge RANS and LES by means of a reduction in the RANS stress tensor, and the transition between them was controlled by the grid size and the Kolmogorov microscale. Baurle et al. [11] proposed a hybrid technique based on a combination of the two-equation k-ω-SST model [12] and the one-equation subgrid-scale turbulent kinetic energy model [11]. Xiao et al. [13] proposed a hybrid technique based on a combination of the two-equation k-ζ (enstrophy) model [14] and the one-equation subgrid-scale turbulent kinetic energy model. Basu et al. [15] proposed a hybrid technique based on a combination of the two-equation k-ε model [16] and the one-equation subgrid-scale turbulent kinetic energy model [17]. Sanchez-Rocha et al. [18] proposed a hybrid technique based on a combination of the two-equation k-ω-SST model [12] and the one-equation localized dynamic subgrid-scale turbulent kinetic energy model [19].

These models used a one-equation subgrid-scale turbulent kinetic energy model in the free shear layers to estimate the velocity scales associated with turbulent eddies. The length scale was estimated based on the grid spacing, as done in early LES work. This deficiency was addressed by Fang and Menon [20,21]; they developed a two-equation subgrid model for the LES of wall-bounded turbulent flow at high Reynolds numbers. This approach, called kinetic eddy simulation (KES), solves for both subgrid kinetic energy k and

Presented as Paper 5216 at the 44th AIAA/ASME/SAE/ASEE Joint Propulsion Conference and Exhibit, Hartford, CT, 21–23 July 2008; received 27 January 2009; revision received 2 February 2010; accepted for publication 2 February 2010.

*Postdoctoral Fellow, School of Aerospace Engineering. Member AIAA.
†Professor, School of Aerospace Engineering. Associate Fellow AIAA.
‡Regents Professor and Associate Chair (Academic), School of Aerospace Engineering. Associate Fellow AIAA.

subgrid length scales l. KES [20,21] has been applied to static stall around a NACA0015 wing, oscillatory attached and dynamic light stall, and dynamic deep stall flows around a NACA0015 airfoil with good agreement with experimental data. Versions of this model have been applied to helicopter rotors in forward flight [22,23].

II. Research Objectives

All of the aforementioned DES and HRLES approaches used a one-equation model in the free shear layers to estimate the velocity scales associated with turbulent eddies, whereas the length scale was estimated based on grid spacing. Therefore, the transition between RANS and LES regions may depend entirely on grid spacing, and it is not correlated with the local flow properties. In the current hybrid Reynolds-averaged Navier–Stokes and kinetic eddy simulation model, this model will be referred to as the hybrid RANS/KES (HRKES) model. This grid-spacing dependency is avoided by using the KES [20,21] model (which computes the length scale l rather than relying on grid spacing Δ) in free shear layers. Furthermore, KES requires using a law-of-the-wall type of approach that requires specifying k and l at the first grid point off the wall. These ad hoc values of k and l at the first grid point off the wall are derived from the analyses of the energy dissipation rate on the wall for attached flows, which might not be suitable for large separated flows or for transonic flows. In the HRKES model, the need to specify k and l is avoided by solving the classical k-ω-SST model equations in near-wall regions, whereas the KES model equations are solved away from walls. This approach provides boundary conditions for both k and l and eliminates the need for any ad hoc specification of their values at the first grid point off the wall, leading to a more robust formulation compared, with using KES everywhere. Thus, the first objective of this study is to determine how to combine the classical k-ω-SST model near walls with the KES model away from walls.

In earlier DES and HRLES approaches, a common difficulty was in determining when and where to switch between near-wall RANS approaches (k-ω or SA) to LES approaches away from walls. In all of the aforementioned DES and HRLES approaches, researchers have used a combination of distance from the wall and grid spacing to switch between these two approaches. In the present study, we invoke the assumption that k and l are continuous functions and blend these quantities estimated from the two approaches. Thus, a second objective of this study is to determine how well this proposed blending works for a variety of external and internal flows.

In the KES model, as in other LES models, the eddy viscosity is proportional to the product of velocity scale k and length scale: Δ in the early LES models and l in the KES model. The constant of proportionality is often specified empirically. In the present study, preliminary efforts have been made to estimate and bound this constant using the realizability constraints [21].

In the following section, the HRKES turbulence model equations are described. Then the present methodology is described and evaluated for flows over airfoils (RAE2822, NACA0015) and a turbine vane configuration.

III. Hybrid RANS/KES Turbulence Model Formulation

This section presents the blended k-ω-SST/KES model equations. In the region close to the wall, Menter's k-ω-SST equations [12] are solved. The present HRKES turbulent kinetic energy equation is formulated as follows,

$$\frac{D(\rho k)}{Dt} = \tau_{ij}\frac{\partial u_i}{\partial x_j} - \frac{k^{\frac{3}{2}}}{l} + \frac{\partial}{\partial x_j}\left[\left(\mu + \frac{\mu_t}{\sigma_k}\right)\frac{\partial k}{\partial x_j}\right] \tag{1}$$

and the k-ω-SST model ω equation [12] is

$$\frac{D(\rho\omega)}{Dt} = \frac{\gamma}{\upsilon_t}\tau_{ij}\frac{\partial u_i}{\partial x_j} - \beta\rho\omega^2 + \frac{\partial}{\partial x_j}\left[\left(\mu + \frac{\mu_t}{\sigma_\omega}\right)\frac{\partial \omega}{\partial x_j}\right] + 2.(1-F_1)\rho\sigma_{\omega_2}\frac{1}{\omega}\frac{\partial k}{\partial x_j}\frac{\partial \omega}{\partial x_j} \tag{2}$$

In the outer region, the k equation is solved as before, and the ω equation is replaced by the kl equation from the KES model [20,21] as follows:

$$\frac{D(\rho(kl))}{Dt} = C_l l\tau_{ij}\frac{\partial u_i}{\partial x_j} - C_{kl}\rho k^{\frac{3}{2}} + \frac{\partial}{\partial x_j}\left[\left(\mu + \frac{\mu_t}{\sigma_{kl}}\right)\frac{\partial (kl)}{\partial x_j}\right] \tag{3}$$

To avoid abrupt jumps in the values of l between near-wall regions and the outer layer, the following blending is used in computing the HRKES length scale:

$$l = F_{\text{blend}}\cdot l_{k\text{-}\omega\text{-SST}} + (1-F_{\text{blend}})\cdot l_{\text{KES}} \qquad l_{k\text{-}\omega\text{-SST}} = \frac{\sqrt{k}}{\beta^*\omega} \tag{4}$$

where l_{KES} is computed from Eq. (3).

Here, the shear stress term is computed from

$$\tau_{ij} = \mu_t\left(\frac{\partial u_i}{\partial x_j} + \frac{\partial u_j}{\partial x_i} - \frac{2}{3}\frac{\partial u_k}{\partial x_k}\delta_{ij}\right) - \frac{2}{3}\rho k\frac{\partial u_i}{\partial x_j} \tag{5}$$

The HRKES model constants are computed from k-ω-SST [12] and KES [20,21] model constants as follows:

$$\sigma_k = F_{\text{blend}}\cdot[\sigma_{k_1}\cdot F_1 + \sigma_{k_2}\cdot(1-F_1)] + (1-F_{\text{blend}})\cdot\sigma_{k_3}$$
$$\sigma_\omega = \sigma_{\omega_1}\cdot F_1 + \sigma_{\omega_2}\cdot(1-F_1) \qquad \beta = \beta_1\cdot F_1 + \beta_2\cdot(1-F_1)$$
$$\gamma = \gamma_1\cdot F_1 + \gamma_2\cdot(1-F_1) \tag{6}$$

where

$$\sigma_{k_1} = 1/0.85, \quad \sigma_{\omega_1} = 2.0, \quad \beta_1 = 0.075, \quad \beta^* = 0.09$$
$$\sigma_{k_2} = 1.0, \quad \sigma_{\omega_2} = 1/0.856, \quad \beta_2 = 0.0828, \quad \sigma_{k_3} = 0.9$$
$$\sigma_{kl} = 2.0, \quad C_l = 1.06, \quad \kappa = 0.41, \quad \gamma_1 = \frac{\beta_1}{\beta^*} - \frac{\kappa^2}{\sigma_{\omega_1}\sqrt{\beta^*}}$$
$$\gamma_2 = \frac{\beta_2}{\beta^*} - \frac{\kappa^2}{\sigma_{\omega_2}\sqrt{\beta^*}} \tag{7}$$

The function F_1 is calculated from

$$F_1 = \tanh\left(\left(\min\left[\max\left[\frac{2\sqrt{k}}{\beta^*\omega y}; \frac{500\nu}{y^2\omega}\right]; \frac{4\rho\sigma_{\omega_2}k}{CD_{k\omega}y^2}\right]\right)^4\right)$$
$$CD_{k\omega} = \max\left[2\rho\sigma_{\omega_2}\frac{1}{\omega}\frac{\partial k}{\partial x_j}\frac{\partial \omega}{\partial x_j}; 10^{-20}\right] \tag{8}$$

The dissipation coefficient of the kl equation is computed as a function of length-scale gradients [21] as follows:

$$C_{kl} = 0.58 + 2\frac{C_\upsilon}{\sigma_{kl}}\left(\frac{\partial l}{\partial x_j}\right)^2 \tag{9}$$

where C_υ is computed following the realizability constraints [21]. Its value has a lower bound that is based on the ratio of turbulent time scale ($t = l/\sqrt{k}$) to shear time scale ($t = 1/\sqrt{(S_{ij}S_{ij} - \frac{1}{3}S_{kk}^2)}$) as follows:

$$C_\upsilon = \min\left[0.0667; \frac{1}{\sqrt{6}}\frac{(\sqrt{k}/l)}{\sqrt{S_{ij}S_{ij} - \frac{1}{3}S_{kk}^2}}\right] \tag{10}$$

Finally, the turbulent viscosity is computed from

Table 1 Options for blending functions and the use of realizability constraints in HRKES

Type	C_υ	F_{blend}
HRKES1	0.0667	F_2 [Eq. (12)]
HRKES2	Equation (10)	F_2 [Eq. (12)]
HRKES3	0.0667	F_1 [Eq. (8)]
HRKES4	Equation (10)	F_1 [Eq. (8)]

$$\mu_t = F_{\text{blend}}\mu_t|_{k\text{-}\omega\text{-SST}} + (1 - F_{\text{blend}})\mu_t|_{\text{KES}}$$
$$\mu_t|_{k\text{-}\omega\text{-SST}} = \frac{0.31\rho k}{\max(0.31\omega; \Omega F_2)} \qquad \mu_t|_{\text{KES}} = C_\upsilon \rho \sqrt{k} l_{\text{KES}} \tag{11}$$

where the function F_2 is computed as follows:

$$F_2 = \tanh\left(\left(\max\left[\frac{2\sqrt{k}}{\beta^* \omega y}; \frac{500\upsilon}{y^2\omega}\right]\right)^2\right) \tag{12}$$

The blending functions studied in the current HRKES model were Menter's k-ω-SST [12] F_1 and F_2 functions. Those distance-dependent blending functions were chosen to ensure a smooth transition between the RANS model in near-wall regions and the LES model away from walls. In the current work, four different options (Table 1) for the HRKES model (a combination of F_1 and F_2 blending functions and the use of realizability constraints to bound the KES model parameters) have been coded, studied, and compared with the classical k-ω-SST turbulence model.

For more details about the k-ω-SST turbulence model, boundary conditions, and initial conditions, the reader is referred to [12]. For more details about the KES turbulence model, boundary conditions, and initial conditions, the reader is referred to [20,21].

IV. Current Methodology

The present studies were done using the in-house solver GT-TURBO3D [24–28]. This solver is a spatially-high-order unsteady three-dimensional compressible flow solver that uses an implicit time-marching scheme and a two-equation k-ω-SST turbulence model. This solver has been extensively validated for helicopter rotors, wind turbines, prop fans, fixed-wing configurations, and single-stage axial and radial compressors [24–27]. As a further validation of this analysis, this solver was also evaluated by Zaki et al. [28] for different single and multistage axial turbine configurations. The code structure, validation studies, and grid convergence studies are documented in the aforementioned references and are not reproduced here, for brevity. The simulations presented here were run until a cyclic convergence was achieved and the solutions were averaged over the converged cycles.

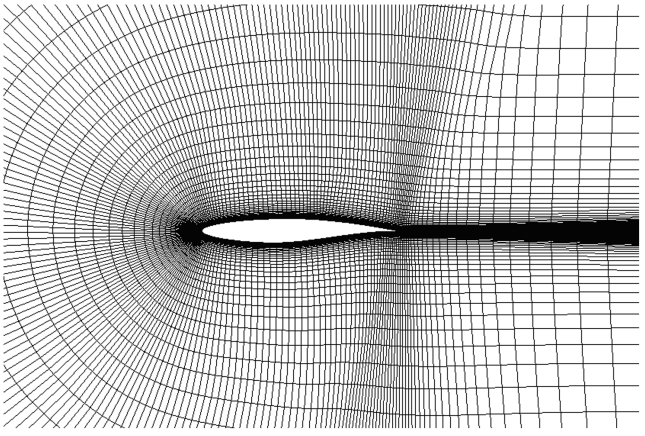

Fig. 1 RAE2822 airfoil (257 × 97 × 5) C-grid.

V. Results and Discussions

The hybrid RANS/KES methodology described above has been applied to a number of internal and external flows (RAE2822 airfoil, NACA0015 airfoil, and a turbine vane configuration). Further description of these cases and the results obtained are described below.

A. RAE2822 Airfoil

The present methodology is applied to a transonic flow over a RAE2822 airfoil. This test case corresponds to test case 10 by Cook

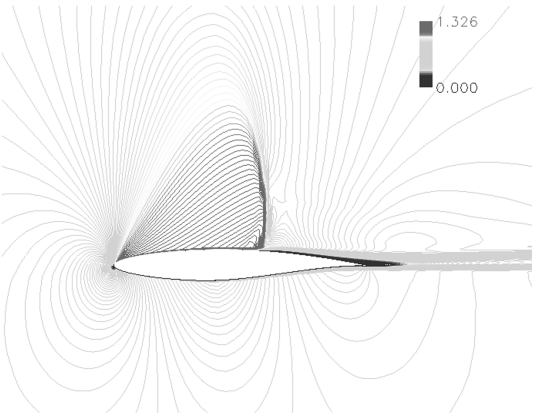

a) k-ω-SST

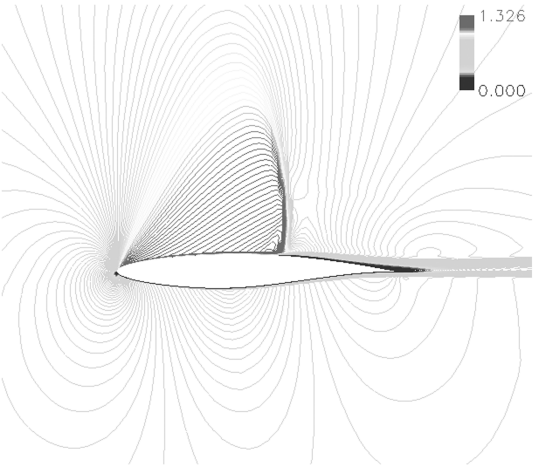

b) HRKES2

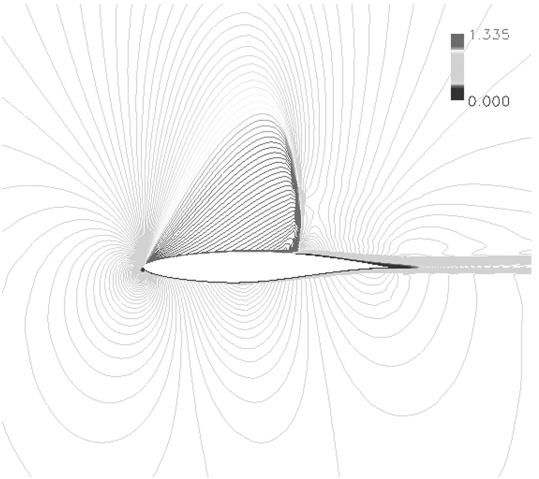

c) HRKES4

Fig. 2 Mach number contours for an RAE2822 airfoil.

et al. [29]. This AGARD standard case was selected because the shock wave was strong enough to induce a boundary-layer separation over the airfoil surface. The flow conditions are a Mach number of 0.75, Reynolds number of 6.2×10^6, and corrected angle of attack of 2.72 deg. This case was simulated using GT-TURBO3D with periodic boundary conditions in the spanwise direction. The grid used in the present computations is a C-grid, which extends 20 chord lengths in all directions. This grid consists of (257 cells in the direction wrapping the airfoil, 97 cells in the normal direction, and 5 cells in the span direction) with 176 cells on the airfoil surface (Fig. 1).

The flowfield around the airfoil was examined through a study of the Mach number contours for all the turbulence models studied. The computed Mach number contours are shown in Fig. 2 (Figs. 2a–2c, for k-ω-SST, HRKES2, and HRKES4, respectively). The solutions of HRKES1 and HRKES3 were similar to HRKES2 and HRKES4, respectively, and are not shown here, for brevity. All the turbulence models were able to capture the shock wave location and the boundary-layer separation caused by the shock wave over the airfoil surface. The smooth Mach number contours indicate that the blending in the HRKES does not introduce any unphysical fluctuations to the flowfield in the buffer zone.

Next, the details of the flow over the airfoil were examined through a comparison of pressure coefficient Cp distributions over the airfoil surface with experimental data [29] for all the turbulence models studied. The computed pressure coefficient distributions are shown in Fig. 3. The computations agree well with experimental data [29]. It is found that the outer-region model has an effect on the near-wall model. It is also found that k-ω-SST, HRKES1, and HRKES2 predicted the shock wave location accurately, whereas HRKES3 and HRKES4 predicted the shock wave location slightly downstream. Furthermore, the solutions with and without using the KES model

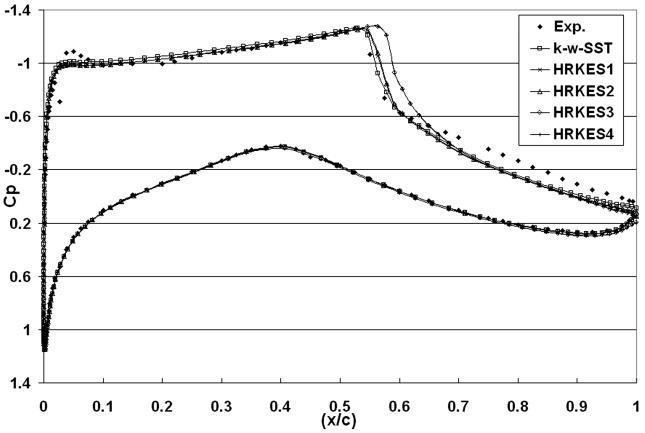

Fig. 3 Pressure coefficient distribution over an RAE2822 airfoil.

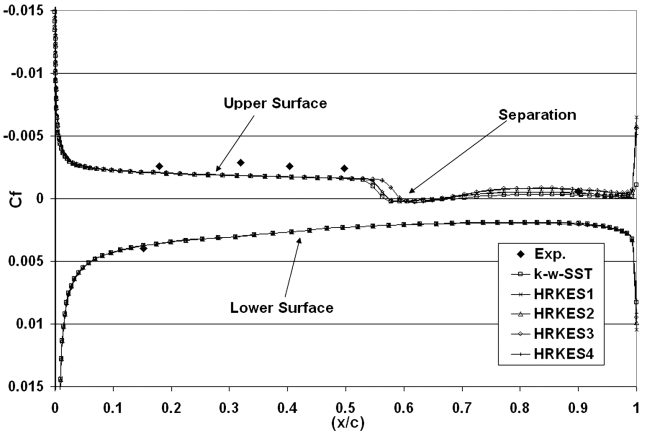

Fig. 4 Skin-friction coefficient distribution over an RAE2822 airfoil.

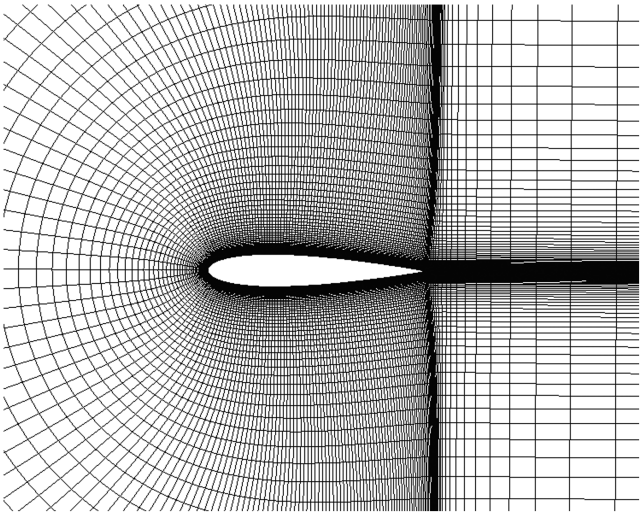

Fig. 5 NACA 0015 airfoil (257 × 129 × 5) C-grid.

realizability constraints were similar, which indicates that those constraints do not impact the solution in the current HRKES model.

Then the skin-friction coefficient C_f distribution over the airfoil was examined and compared with experimental data [29], as shown in Fig. 4. The computational results agree well with the experiments. The separation induced by the shock wave on the upper surface of the airfoil is accurately captured by all the turbulence models studied.

A grid independency study was also done for this case and the pressure and skin-friction coefficients over the airfoil obtained using the different grid densities were similar and are not shown here, for brevity, but can be found in [30].

B. NACA0015 Airfoil

To further explore the differences between the HRKES and the k-ω-SST turbulence models, the flowfield over a NACA0015 airfoil was studied at different high angles of attack. This test case corresponds to the test case by Piziali [31]. The flow conditions are Mach number of 0.289 and Reynolds number of 1.94×10^6. This case was simulated using GT-TURBO3D with periodic boundary conditions in the spanwise direction. The C-grid used in the present computations consists of 257 cells in the direction wrapping the airfoil, 129 cells in the normal direction, and five cells in the span direction, as shown in Fig. 5.

The lift-coefficient values for this airfoil at different angles of attack using the HRKES model different options and the k-ω-SST model are compared with the experimental data [31] in Fig. 6. The experimental data has more points than the computational data at high angles of attack; this is because the experimental measurements were obtained while the airfoil was slowly pitched up and down,

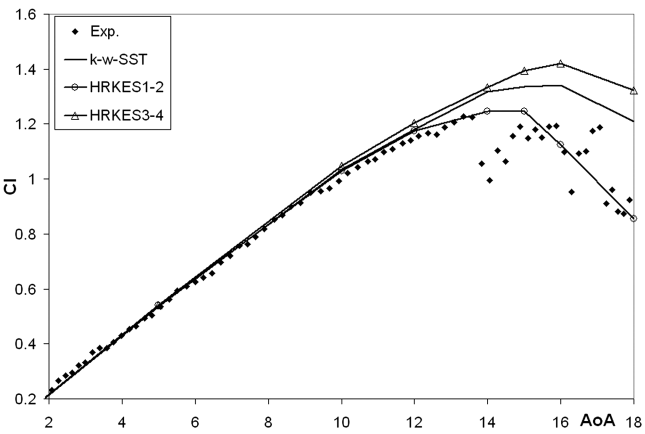

Fig. 6 Lift coefficient vs angle of attack for NACA0015 airfoil.

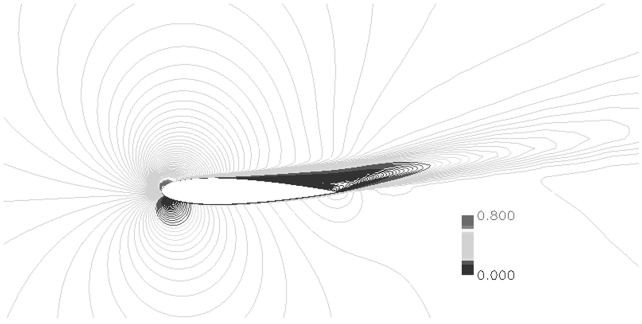

a) k-ω-SST

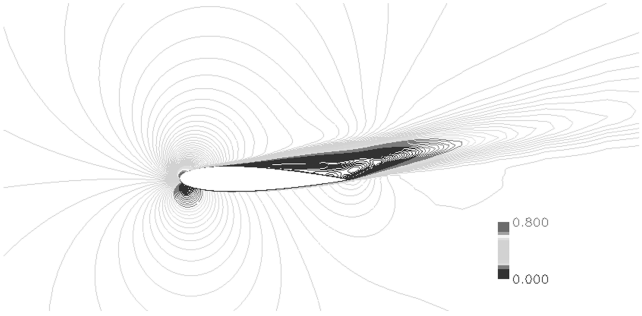

b) HRKES2

Fig. 7 Mach number contours for NACA0015 at a 16 deg angle of attack.

whereas the computational data were obtained by fixing the airfoil at different angles of attack. The computational results agree well with the experimental results for all the turbulence models studied. It is found that the HRKES1 and HRKES2 predicted the lift-coefficient values better than the baseline k-ω-SST model at higher angles of attack. Also, HRKES1 and HRKES2 predicted the stall onset at an angle of attack of around 14 deg, whereas the k-ω-SST model predicted it at around 16 deg. It is also found that HRKES3 and HRKES4 predicted higher lift-coefficient values than the k-ω-SST, HRKES1, and HRKES2 models at higher angles of attack. This shows that the fidelity of the hybrid RANS/LES turbulence models depend on the underlying blending functions. Furthermore, the solutions with and without using the KES model realizability constraints were similar, which indicates that the realizability constraints have a minor role in the current HRKES model.

Next, the flowfield around the airfoil at high angles of attack was examined through a study of the Mach number contours. The computed Mach number contours for both k-ω-SST and HRKES2 turbulence models are shown in Fig. 7 for the case with a 16 deg angle of attack. The smooth Mach number contours indicate that the blending in the HRKES model does not introduce any unphysical fluctuations to the flowfield in the buffer zone for large separated flowfields.

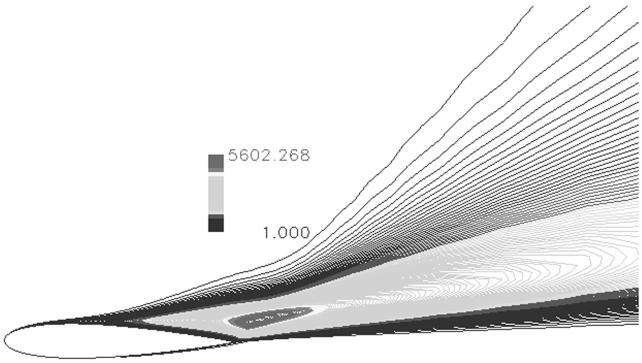

a) k-ω-SST

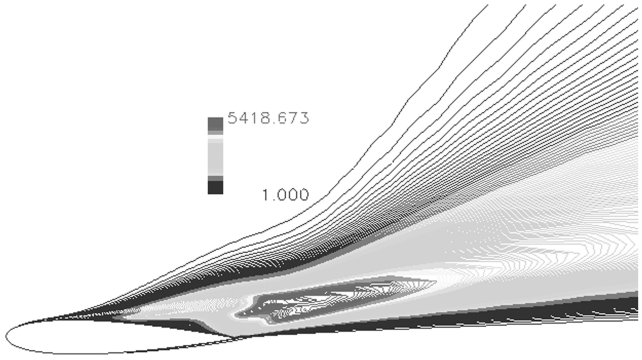

b) HRKES2

Fig. 8 Viscosity contours for NACA0015 at a 16 deg angle of attack.

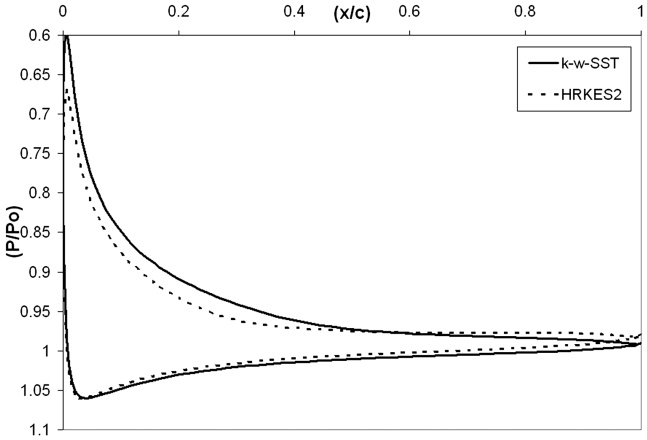

Fig. 9 Pressure distribution over NACA0015 at a 16 deg angle of attack.

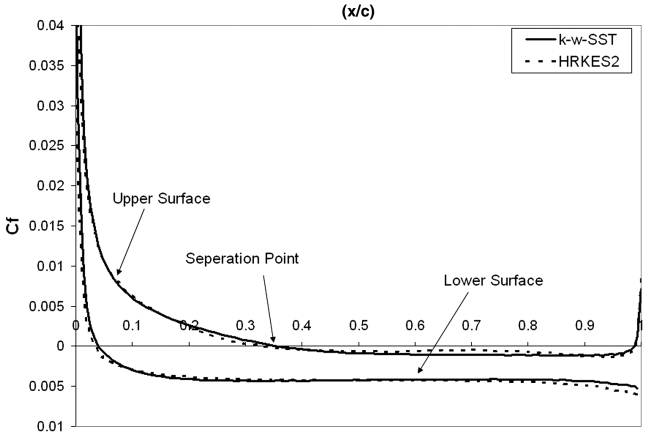

Fig. 10 Skin-friction coefficient distribution over NACA0015 at a 16 deg angle of attack.

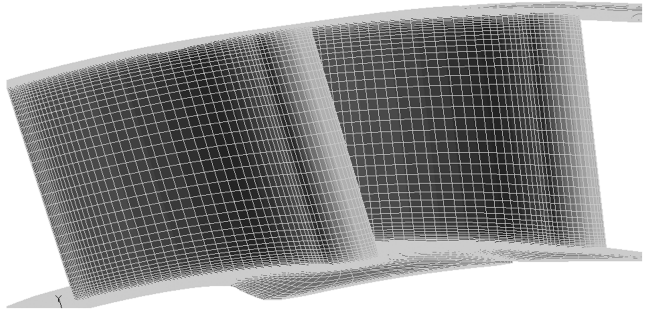

Fig. 11 Goldman turbine vane (137 × 63 × 32) C-grid.

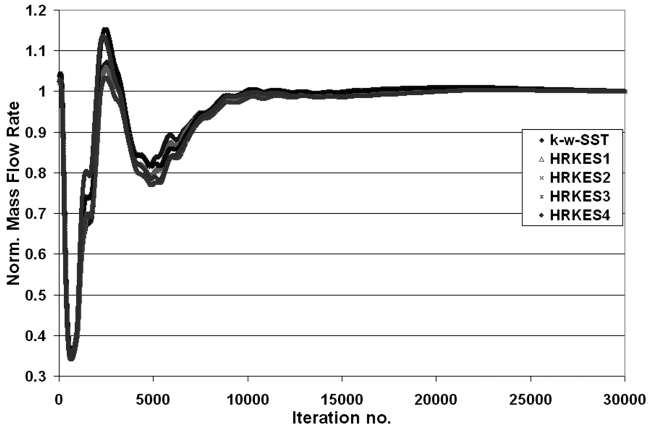

Fig. 12 Nondimensional mass-flow-rate convergence history for Goldman turbine vane.

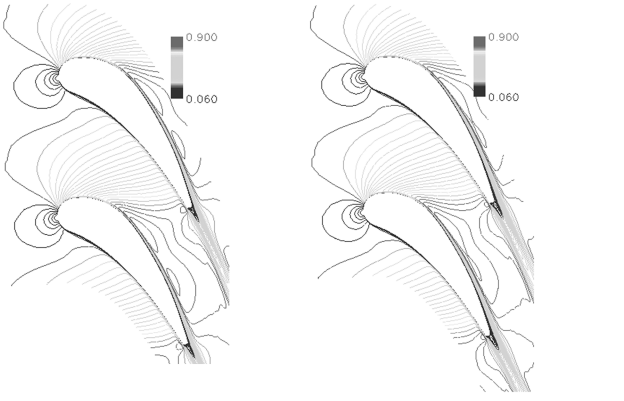

a) k-w-SST **b) HRKES1**

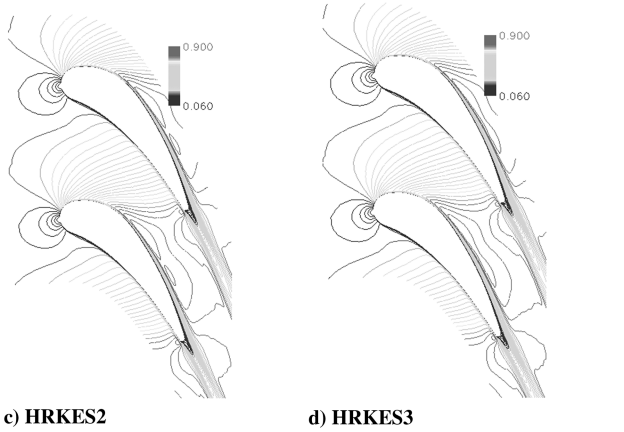

c) HRKES2 **d) HRKES3**

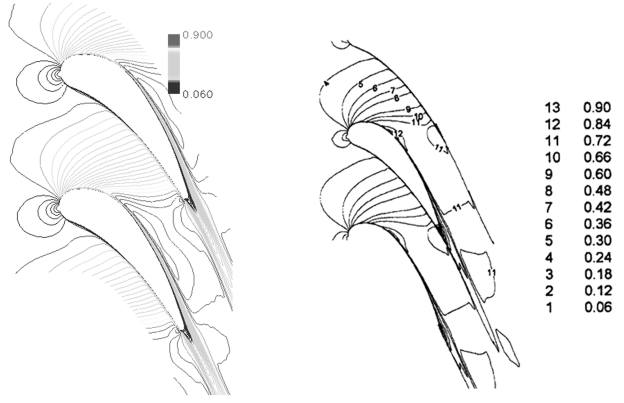

e) HRKES4 **f) Yeuan et al. [34]**

Fig. 13 Mach number contours at midspan for Goldman turbine vane.

The flowfield viscosity contours (as a multiplication of the laminar viscosity) around the airfoil at an angle of attack of 16 deg are shown in Fig. 8. It is shown that the k-ω-SST model predicted higher viscosity levels than the HRKES2 model. It is also shown that high viscosity levels predicted by the k-ω-SST model are denser than those predicted by the HRKES2 model.

Then the details of the flow over the airfoil were examined through a comparison of pressure distribution and skin-friction coefficient C_f distribution over the airfoil surface for both k-ω-SST and HRKES2 turbulence models. The computed pressure distribution and skin-friction coefficient distribution are shown in Figs. 9 and 10, respectively, for the case with a 16 deg angle of attack. It is found that the outer-region model has an effect on the near-wall model. It is shown that the k-ω-SST underpredicted the pressure over the airfoil's upper-half surface compared with HRKES2, which led to the overpredictions in the lift-coefficient values compared with HRKES2. No large differences found in the skin-friction coefficient over the airfoil surface between k-ω-SST and HRKES2 turbulence models.

C. Goldman Turbine Vane

The present methodology is applied to an annular turbine stator that was developed and tested at NASA John H. Glenn Research Center at Lewis Field by Goldman and McLallin [32]. This stator has 36 vanes. The vanes have an axial chord length of 0.03823 m, a span (between the hub and the tip) of 0.0381 m, a 0.508 m tip diameter, and a hub-to-tip radius ratio of 0.85. The inlet Mach number is 0.211. It has a design pressure ratio of 0.6705, exit Mach number of 0.665, and Reynolds number based on the axial chord of 173,000. A C-grid with 137 cells in the direction wrapping the blade, 63 cells in the radial direction, and 32 cells in the blade-to-blade direction was used in this study, as shown in Fig. 11. This grid was generated using the grid generator TCGRID developed by Chima [33]. Figure 12 shows the convergence history of the normalized mass flow rate for all the turbulence models studied. It is found that all of the four options listed in Table 1 have good convergence characteristics, similar to the baseline k-ω-SST model, and that they all converged after approximately 20,000 iterations to the designed mass flow rate.

Next, the flowfield inside the stator passage was examined through a study of Mach number contours and comparison with published computational results [34] for the same configuration on a comparable grid. The Mach number contours at 50% span from hub are shown in Fig. 13; they show very good agreement with the published computational results [34]. This indicates that the transition between the near-wall k-ω-SST model and the outer-region KES model is smooth and does not introduce any noise or fluctuations to the flowfield in the buffer region.

Next, the details of the flow over the blades were examined through a comparison of pressure distributions over the stator blade surface with experimental data [32]. Normalized surface pressure distributions at 50% span from hub are shown in Fig. 14. The computed solution agrees very well with experimental data [32] over

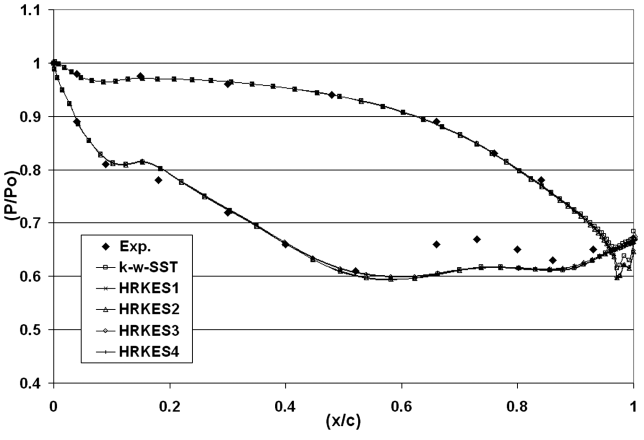

Fig. 14 Surface pressure distributions at midspan for Goldman turbine vane.

most of the blade surface, except for slight discrepancies over the upper blade surface aft of 75% of the chord. It is found that all the turbulence models studied here predicted almost identical Mach number contours and blade surface pressure distributions, indicating that for completely attached flows; the HRKES model is almost identical to the k-ω-SST model.

VI. Conclusions

A hybrid RANS/KES turbulence model is developed for external and internal flow applications. This HRKES model solves Menter's k-ω-SST model near walls and switches to the KES model away from walls. Within this HRKES model, a combination of two blending functions and the use of realizability constraints to bound the KES model parameters have been evaluated and then applied to a number of internal and external flows (RAE2822 airfoil, NACA0015 airfoil, and a turbine vane configuration). It is found that the HRKES model is more robust than the KES model alone and converges reliably for 2-D and 3-D configurations. For completely attached flows, the HRKES model was almost identical to the k-ω-SST model. Solutions with and without using the KES model realizability constraints were similar, indicating that those realizability constraints mostly impact the near-wall regions, which are dominant by the RANS model in the current HRKES approach. Blending k-ω-SST with KES using the k-ω-SST F_2 function showed better predictions in separated flows than the k-ω-SST model. More work is needed to estimate the KES model constants dynamically and to develop a hybrid adaptive switching between k-ω-SST and KES models.

References

[1] Piomelli, U., and Chasnov, J. R., "Large-Eddy Simulations: Theory and Applications," *Transition and Turbulence Modeling*, edited by D. Henningson, M. Hallbäck, H. Alfredsson, and A. Johansson, Kluwer Academic, Dordrecht, The Netherlands, 1996, pp. 269–336.

[2] Smith, A. M. O., and Cebeci, T., "Numerical Solution of the Turbulent Boundary Layer Equations," Douglas Aircraft, Rept. 33735, Berkeley, MO, 1967.

[3] Baldwin, B. S., and Lomax, H., "Thin-Layer Approximation and Algebraic Model for Separated Turbulent Flows," AIAA Paper 1978-257, 1978.

[4] Spalart, P. R., Jou, W. H., Strelets, M., and Allmaras, S. R., "Comments on the Feasibility of LES for Wings, and on a Hybrid RANS/LES Approach," *Proceedings of the First AFOSR International Conference on DNS/LES*, Ruston, LA, 1997.

[5] Spalart, P. R., and Allmaras, S. R., "A One-Equation Turbulence Model for Aerodynamic Flows," *La Recherche Aerospatiale: Bulletin Bimestriel de l'Office National d'Etudes et de Recherches Aerospatiales*, Vol. 1, 1994, pp. 5–21; also AIAA Paper 92-0439, 1992.

[6] Strelets, M., "Detached Eddy Simulation of Massively Separated Flows," 39th AIAA Aerospace Sciences Meeting and Exhibit, AIAA Paper 2001-0879, 2001.

[7] Nichols, R. H., "Comparison of Hybrid RANS/LES Turbulence Models on a Circular Cylinder at High Reynolds Number," 43rd AIAA Aerospace Sciences Meeting and Exhibit, AIAA Paper 2005-498, Reno, NV, 2005.

[8] Basu, D., Hamed, A., and Das, K., "DES and Hybrid RANS/LES Models for Unsteady Separated Turbulent Flow Predictions," AIAA Paper 2005-0503.

[9] Nichols, S., Sreenivas, K., Karman, S., and Mitchell, B., "Turbulence Modeling for Highly Separated Flows," 45th AIAA Aerospace Sciences Meeting and Exhibit, AIAA Paper 2007-1407, Reno, NV, Jan. 2007.

[10] Speziale, C. G., "Turbulence Modeling for Time Dependent RANS and VLES: A Review," *AIAA Journal*, Vol. 36, No. 2, 1998, pp. 173–184. doi:10.2514/2.7499

[11] Baurle, R. A., Tam, C. J., Edwards, J. R., and Hassan, H. A., "Hybrid Simulation Approach for Cavity Flows: Blending, Algorithm, and Boundary Treatment Issues," *AIAA Journal*, Vol. 41, No. 8, 2003, pp. 1463–1480. doi:10.2514/2.2129

[12] Menter, F. R., "Two-Equation Eddy-Viscosity Turbulence Models for Engineering Applications," *AIAA Journal*, Vol. 32, No. 8, 1994, pp. 1598–1605. doi:10.2514/3.12149

[13] Xiao, X., Edwards, J. R., and Hassan, H. A., "Blending Functions in Hybrid Large-Eddy/Reynolds-Averaged Navier- Stokes Simulations," *AIAA Journal*, Vol. 42, No. 12, 2004, pp. 2508–2515. doi:10.2514/1.2094

[14] Robinson, D. F., and Hassan, H. A., "Further Development of the k-ζ (Enstrophy) Turbulence Closure Model," *AIAA Journal*, Vol. 36, No. 10, 1998, pp. 1825–1833. doi:10.2514/2.298

[15] Basu, D., Hamed, A., Das, K., and Tomko, K., "Comparative Analysis of Hybrid Turbulence Closure Models in the Unsteady Transonic Separated Flow Simulations," 44th AIAA Aerospace Sciences Meeting and Exhibit, AIAA Paper 2006-117, Reno, NV, 9–12 Jan. 2006.

[16] Jones, W. P., and Launder, B. E., "The Prediction of Laminarization with a Two-Equation Model of Turbulence," *International Journal of Heat and Mass Transfer*, Vol. 15, 1972, pp. 301–313. doi:10.1016/0017-9310(72)90076-2

[17] Yoshizawa, A., and Horiuti, K., "A Statistically Derived Subgrid Scale Kinetic Energy Model for the Large-Eddy Simulation of Turbulent Flows," *Journal of the Physical Society of Japan*, Vol. 54, No. 8, 1985, pp. 2834–2839. doi:10.1143/JPSJ.54.2834

[18] Sanchez-Rocha, M., Kirtas, M., and Menon, S., "Zonal Hybrid RANS-LES Method for Static and Oscillating Airfoils and Wings," 44th AIAA Aerospace Sciences Meeting and Exhibit, AIAA Paper 2006-1256, Reno, NV, Jan. 2006.

[19] Menon, S., and Kim, W., "A New Dynamic One-Equation Subgrid Model for Large-Eddy Simulations," AIAA Paper 1995-0356.

[20] Fang, Y., and Menon, S., "A Two Equation Subgrid Model for Large Eddy Simulation of High Reynolds number Flows," 44th AIAA Aerospace Sciences Meeting and Exhibit, AIAA Paper 2006-116, Reno, NV, 9–12 Jan. 2006.

[21] Fang, Y., and Menon, S., "Kinetic Eddy Simulation of Static and Dynamic Stall," 24th Applied Aerodynamics Conference, AIAA Paper 2006-3847, San Francisco, 5–8 June 2006.

[22] Shelton, A., Braman, K., Smith, M., and Menon, S., "Improved Hybrid RANS-LES Turbulence Models for Rotorcraft," *AHS 62nd Annual Forum* [CD-ROM], AHS International, Alexandria, VA, May 2006.

[23] Duque, E. P. N., Sankar, L. N., Menon, S., Ruffin, S., Smith, M., Ahuja, A., Brentner, K. S., Long, L. N., Morris, P. J., and Gandhi, F., "Revolutionary Physics-Based Design Tools for Quiet Helicopters," 44th AIAA Aerospace Sciences Meeting and Exhibit, AIAA Paper 2006-1068, Reno, NV, 9–12 Jan. 2006.

[24] Stein, A., Niazi, S., and Sankar, L. N., "Computational Analysis of the Centrifugal Compressor Surge Control Using Air Injection," *Journal of Aircraft*, Vol. 38, No. 3, May–June 2001, pp. 513–520. doi:10.2514/2.2791

[25] Stein, A., Niazi, S., and Sankar, L. N., "Computational Analysis of Surge and Separation Control in Centrifugal Compressors," *Journal of Propulsion and Power*, Vol. 16, No. 1, January–February 2000, pp. 65–71. doi:10.2514/2.5532

[26] Niazi, S., Stein, A., and Sankar, L. N., "Computational Analysis of Stall Control Using bleed Valve in a High-Speed Compressor," 36th AIAA Joint Propulsion Conference, AIAA Paper 2000-3507, Huntsville, AL, 2000.

[27] Niazi, S., Stein, A., and Sankar, L. N., "Numerical Studies of Stall and Surge Alleviation in a High-Speed Transonic Fan Rotor," 38th AIAA Aerospace Sciences Meeting, AIAA Paper 2000-0225, Reno, NV, 2000.

[28] Zaki, M., Iyengar, V., and Sankar, L. N., "Assessment of Rotor-Stator Interface Boundary Condition Techniques for Modeling Axial Flow Turbines," 42nd AIAA/ASME/SAE/ASEE Joint Propulsion Conference and Exhibit, AIAA Paper 2006-4619, Sacramento, CA, July 2006.

[29] Cook, P. H., McDonald, M. A., and Firmin, M. C. P., "Aerofoil RAE 2822—Pressure Distributions, and Boundary Layer and Wake Measurements," Experimental Data Base for Computer Program Assessment, AGARD Rept. AR 138, 1979.

[30] Zaki, M., "Physics Based Modeling of Axial Compressor Stall," Ph.D. Dissertation, School of Aerospace Engineering, Georgia Inst. of Technology, Atlanta, Dec. 2009.

[31] Piziali, R. A., "2-D and 3-D Oscillating Wing Aerodynamics for a Range of Angles of Attack Including Stall," NASA TM-4632, 1994.

[32] Goldman, L. J., and McLallin, K. L., "Cold Air Annular Cascade Investigations of Aerodynamic Performance of Core-Engine-Cooled Turbine Vanes. 1: Solid Vane Performance and Facility Description," NASA TM X-3224, 1975.

[33] Chima, R. V., *TCGRID 3-D Grid Generator for Turbomachinery*, July 2003.

[34] Yeuan, J. J., and Hamed, A., "Three Dimensional Viscous Flow Simulations in a Turbine Stator Using a Nonperiodic H-Typed Grid," AIAA Paper 1998-3562.